Eur. J. Mineral., 35, 383–395, 2023
https://doi.org/10.5194/ejm-35-383-2023

European Journal of Mineralogy
Open Access

Supergene phases from ferruginous duricrusts: non-destructive microsampling and mineralogy prior to (U–Th) / He geochronological analysis

Karina P. P. Marques[1,2], Thierry Allard[2], Cécile Gautheron[3], Benoît Baptiste[2], Rosella Pinna-Jamme[3], Guillaume Morin[2], Ludovic Delbes[2], and Pablo Vidal-Torrado[1]

[1]"Luiz de Queiroz" College of Agriculture, University of São Paulo, 13418-900, Piracicaba, São Paulo, Brazil
[2]Institut de Minéralogie, de Physique des Matériaux et de Cosmochimie, UMR CNRS 7590, Sorbonne Université, IRD, MNHN, 75252, Paris CEDEX 05, France
[3]Université Paris-Saclay, CNRS, GEOPS, 91405, Orsay, France

Correspondence: Karina P. P. Marques (karina.marques@alumni.usp.br)

Received: 30 August 2022 – Revised: 8 March 2023 – Accepted: 15 March 2023 – Published: 14 June 2023

Abstract. Interpreting the ages of supergene mineralogical phases in laterite is complex because they consist of polycrystalline mixtures of different phases at the microscopic scale that could be crystalized at different epochs. Among the geochronometers, the (U−Th)/He method on hematite and goethite is more often used, but ages can be difficult to interpret due to phases mixing. To resolve this issue, this study proposes a methodology for performing detailed mineralogical analysis of hematite and goethite single grains prior to their dating using the (U−Th)/He method. Strictly non-destructive mineralogy of single grains is not achievable by classical tools, such as conventional powder XRD (X-ray diffraction; requiring at least some milligrams of powder) or SEM (scanning electron microscopy; that can contaminate the grain by coating or fixing). Therefore, we performed X-ray diffraction patterns of single grains using high-flux X-ray beams from both a rotating anode (XRD_rotat) laboratory diffractometer and a synchrotron beamline (XRD_synch) and compared the results in order to design a method based on XRD_rotat only. For this purpose, two samples from the pisolitic facies of a Brazilian ferruginous duricrust (Alto Paranaíba region, Minas Gerais State, Brazil) were chosen because they presented a usual heterogeneity. Rietveld refinements of the XRD patterns obtained from both XRD_rotat and XRD_synch yielded similar results for the weight percentage ratio of the main phases and mean coherent domain sizes and less similar results for Al substitution rates, thus validating the XRD_rotat approach. No beam damage was observed when increasing X-ray exposure time, neither on XRD patterns nor on (U−Th)/He ages. Hence, submillimeter, undisturbed grains can be used to analyze the mineralogy of ferruginous duricrusts by XRD_rotat with a short exposure, and the same grains can subsequently be dated by (U−Th)/He geochronology analysis. The (U−Th)/He dating of pisolitic core and cortex grains also provided meaningful ages: they revealed two evolution phases of the ferruginous duricrust, which occurred at or before the Oligocene for the pisolitic core and middle Miocene for the pisolitic cortex, agreeing with the previous model for the development of pisolites. The mineralogy of single grains selected for dating is helpful for discussing the crystallization ages, and the high-flux XRD approach may be applied to other supergene mineral parageneses used for absolute dating.

Published by Copernicus Publications on behalf of the European mineralogical societies DMG, SEM, SIMP & SFMC.

1 Introduction

Ferruginous duricrusts, containing hematite and/or goethite as major components, consist of hard iron-rich horizons formed at or near the ground surface of laterites that are widespread in intertropical areas (e.g., Tardy, 1993; Tardy and Roquin, 1998). Their modes of formation have been extensively discussed in order to unravel the complexity arising from their polyphasic nature (e.g., McFarlane, 1976; Nahon, 1986, 1991; Tardy, 1993; Tardy and Roquin, 1998; Ollier and Sheth, 2008). In the landscape, they may represent paleosurfaces that partially resisted erosion and weathering for long periods, as well as extend as far back as the Mesozoic (e.g., Shuster et al., 2012; Beauvais and Chardon, 2013; Monteiro et al., 2018; Vasconcelos and Carmo, 2018; Vasconcelos et al., 2019). In order to understand and reconstruct related continental surface evolution through time as a result of geodynamic or paleoclimate forcing, it is necessary to perform absolute dating of appropriate mineral components of ferruginous duricrusts, such as goethite and hematite (Théveniaut and Freyssinet, 1999, 2002; Shuster et al., 2005; Monteiro et al., 2014; Allard et al., 2018; Vasconcelos et al., 2019). Through (U−Th)/He geochronology, the knowledge on their timing of formation is continuously increasing, but the chronology of ancient landscapes worldwide in relation to paleoclimatic events is still fragmented and remains a topical issue (Shuster et al., 2005, 2012; Vasconcelos et al., 2013; Monteiro et al., 2014; Allard et al., 2018; Monteiro et al., 2018; Heller et al., 2022; Gautheron et al., 2022).

In the (U−Th)/He dating methodology, sample mineralogy is analyzed using conventional X-ray diffraction (XRD) and scanning electron microscopy (SEM) on facies recognized at the millimeter (color and texture) to micrometer scale. However, the small size of iron oxides and oxyhydroxide crystallites (typically less than 1 µm) implies that sub-millimeter grains used for dating (typically less than 500 µm large) can be polycrystalline. Thus, they may exhibit a mineralogical composition that is different from that of the sample otherwise analyzed with conventional XRD or SEM. This may induce some bias when interpreting and discussing the (U−Th)/He results, especially when goethite and hematite exhibit contrasting ages according to the sub-millimeter sampled facies (Anand and Gilkes, 1987). In addition, He retention is slightly different in hematite and goethite, leading to correction of the (U−Th)/He age (e.g., Shuster et al., 2005). For hematite, values of a few percentage points ($\sim 1\,\%$ to $5\,\%$) have been proposed to correct the (U−Th)/He ages from He loss by diffusion, depending on crystallite sizes and He diffusion coefficient (Lippolt et al., 1994; Farley and Flowers, 2012; Evenson et al., 2014; Balout et al., 2017; Farley, 2018). By contrast, for goethite, He loss correction factors ranging from some percentage points (Hofmann et al., 2017) to 10 %–30 % (Deng et al., 2017; Heim et al., 2006; Shuster et al., 2005) that correlate with the radioactive damage dose and Al content (Bassal et al., 2022) have been proposed. In addition, having access to the mineralogy of the dated grains will allow one to get a better He loss characterization and to identify possible hematite–goethite phase mixing leading to dispersed (U−Th)/He ages (Monteiro et al., 2014; Heller et al., 2022).

Classical mineralogical investigations cannot be performed easily on the same sample as the one used for (U−Th)/He dating: environmental SEM may avoid contamination of the grains, but one gets a 2D slice, making volume fractions of phases difficult to estimate. In addition, the different oxides are not easily distinguished, either by backscatter electrons or by energy-dispersive spectrometer (EDS). Micro-Raman provides contrasting spectra for hematite or goethite, but it would certainly require appropriate references to allow for quantitative mineralogy. Conventional XRD requires sample mass (at least several milligrams of powder) much higher than that of a single grain extracted for (U−Th)/He dating. Consequently, in order to support interpretation and discussion of (U−Th)/He ages of iron oxide and oxyhydroxide generations from ferruginous duricrusts with mineralogy, it appears critical to analyze the same single grain that will be subsequently used for (U−Th)/He dating. Aliquot-specific mineralogical data are of prime importance because in the case of mixtures, the hematite and goethite may have different ages, so the mineralogical composition may help in discussing the average ages of the samples. Subsequently, this should have implications on the conditions of formation of the duricrust and then on climatic forcing. Undisturbed single grain analysis can be potentially achieved using a powerful source of X-rays that is far beyond classical setups, such as those available from a rotating anode (XRD_rotat) in a laboratory or a synchrotron (XRD_synch).

Consequently, the present study's objectives are twofold. First, we propose to refine the mineralogical characterization of Fe-oxides and oxyhydroxides from ferruginous duricrusts on sub-millimeter (ca. 500 µm), undisturbed grains prior to dating the same grains by (U−Th)/He method. On two contrasting natural samples from a Brazilian pisolitic duricrust (Alto Paranaíba region, Minas Gerais State), the XRD_rotat patterns are compared to the better-resolved XRD_synch patterns. Related data allowed us to determine parameters that are useful to recognize distinct generations of iron phases (i.e., mean coherent domain (MCD) sizes and Al substitution rate) and the weight percentage (wt %) ratio of the main phases using Rietveld refinement analysis (Bish and Post, 1993). Indeed, Al is a typical substitutional impurity in hematite (up to 15 mol %) and goethite (up to 33 mol %) and thus is due to specific conditions of formation, for example related to the dissolution of kaolinite while the iron oxide crystallizes (Schwertmann et al., 1979; Schulze, 1984). Consequently, the Al substitution rate can define different populations of Fe-oxides that can be subsequently dated by the (U−Th)/He method and potentially be assimilated as distinct generations. The MCD size is fully related to the diffraction process and should be regarded as the minimum

grain size, as a crystallite may potentially contain several MCDs separated by extended defects. In addition, Al content in goethite influences the He retention and the correction factor (Bassal et al., 2022). Second, using this methodology, the (U−Th)/He ages of the cortex and core of the pisolitic samples were determined and discussed as an example. Pisolites are frequently observed in lateritic ferruginous duricrusts, may exhibit contrasting mineralogy between the core and cortex, and are thus relevant for the two objectives of this study. This methodology is shown to be appropriate to identify and quantify different Fe-oxides and oxyhydroxides in dated grains and also potentially to reveal mineral contaminants.

2 Material and methods

2.1 Sampling site

A lateritic ferruginous duricrust profile (∼ 1100 m elevation) developed on relict low-relief uplands in the tropical Brazilian continental interior, Alto Paranaíba region (Minas Gerais State, Brazil), was chosen for sampling (Fig. 1). It is formed at the expense of pyroclastic and epiclastic rocks from the Mata da Corda group (upper Cretaceous) (CPRM, 2014). Despite being an important tropical Brazilian area of occurrence of thick lateritic profiles including duricrusts (Marques et al., 2021), no weathering geochronological data are available yet. The climate of the study area is Aw (Köppen–Geiger's classification), characterized by warm and dry winters and moist and warm summers. The average annual rainfall is 1600 mm, and the mean annual temperature is 22 °C (Oliveira et al., 2020).

The morphological description of the profile was carried out based on McFarlane (1976), Tardy (1993), and Aleva (1994), and then non-disturbed samples were taken from all the described layers. Based on the morphological description at the fieldwork and laboratory, the pisolitic facies, which is often encountered in lateritic ferruginous duricrusts (Nahon, 1991; Tardy, 1993), was chosen due to being structurally suitable for dating, and also because it presented a usual complexity or heterogeneity allowing us to carry out our methodological approach.

2.2 Selection and preparation of samples

The morphological characteristics of a hand specimen from the pisolitic facies were observed and described using a binocular microscope. The populations of Fe-oxides were identified based on texture, color, and morphology (Tardy, 1993), and then the pisolites were isolated. The semi-quantitative composition of a complete pisolite was analyzed by a Zeiss Ultra55 SEM with a FEG-Schottky electronic source coupled with an EDS. The working distance was 19.6 mm, and the acceleration voltage was 15 kV.

Another pisolite with similar morphological characteristics and belonging to the same identified population was sampled using a diamond micro-drill to divide the cortex and core. Grains (ca. 500 µm large) were carefully selected from the cortex and core using an optical microscope. Some of the grains were prepared by hand grinding using a mortar and pestle and then homogenized and sieved at 100 µm in order to obtain powder samples (∼ 0.50 mg). In the other selected grains (∼ 0.10 mg), no preparation was carried out.

2.3 X-ray diffraction data collection and analysis

Both powder samples and single polycrystalline grain samples from the pisolitic cortex and core were analyzed for their mineralogical composition using XRD. Samples were loaded in borosilicate capillaries either as powder fillings or as inserted grains. Laboratory X-ray experiments were performed at the X-ray diffraction platform of the Institut de Minéralogie, de Physique des Matériaux et de Cosmochimie (IMPMC), Sorbonne Université (Paris, France). The single polycrystalline grain samples from the pisolitic core were first analyzed using a Panalytical XpertPro MPD two-circle diffractometer (Co sealed tube in Debye–Scherrer transmission geometry – $\lambda K\alpha 1 = 1.789010$ Å, $\lambda K\alpha 2 = 1.792900$ Å – at 45 keV and 40 mA, with a range scan of 3–90° 2θ and a step size of 0.03° 2θ s^{-1}). The signal collected from the grain was too low, even after several hours of exposure, and even the powder in the capillary exhibited noise after 15 h counting (Fig. S1 in the Supplement). Therefore, more intense and collimated sources were required to analyze small grains in transmission geometry.

A Rigaku MM007HF diffractometer equipped with Varimax focusing optics, a RAXIS4++ image plate detector placed at a distance of 200 mm from the sample, and a Mo rotating anode ($\lambda K\alpha 1 = 0.709319$ Å and $\lambda K\alpha 2 = 0.713609$ Å) at 50 keV and 24 mA were used, with a range scan of 3 to 45° 2θ and the acquisition time of 60 min. The Fit2D program (Hammersley, 2016) was used for the integration of 2D images into 1D patterns after a calibration with LaB6 standard. Rotating anode generators are one of the most powerful X-ray sources available in the laboratory. In these experimental settings operating under a high vacuum, a cooled rotating surface is continuously irradiated by an intense electron beam (Fig. 2), resulting in an improved signal-to-noise ratio and in the possibility to analyze small samples.

Higher X-ray fluxes require the use of a synchrotron beamline. Therefore, XRD_synch patterns were collected on the same grains at the CRISTAL beamline of the SOLEIL Synchrotron (Saint-Aubin, France). We used the two-circle diffractometer of the CRISTAL beamline equipped with a MYTHEN2 X 9K detector (DECTRIS). The measurements were performed in continuous mode at 17 keV (0.72896 or 0.727913 Å) using 5 min exposure time, with a scan range of 3–65° 2θ and a scan speed of 0.04° 2θ s^{-1}.

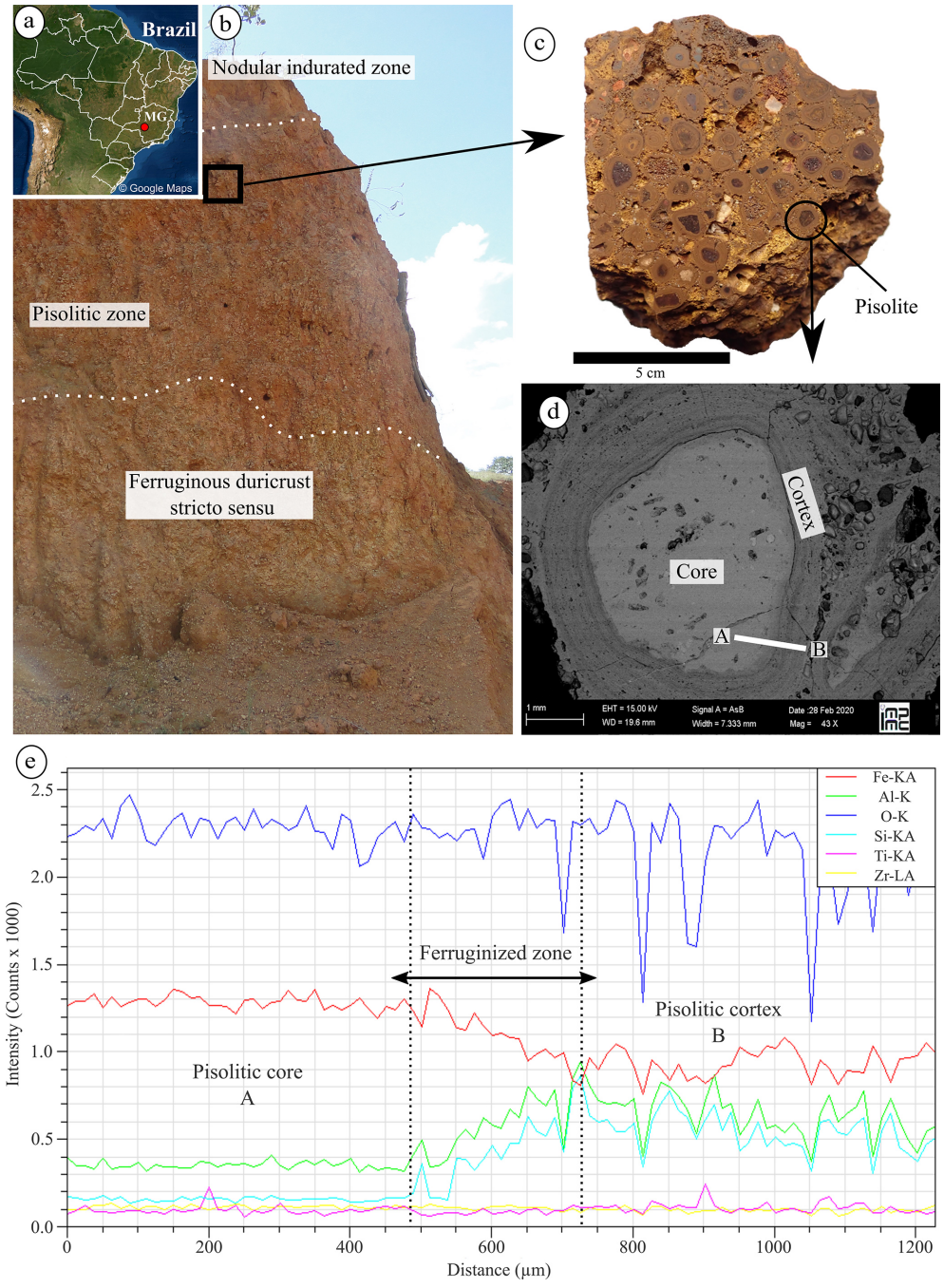

Figure 1. Ferruginous duricrust profile and pisolitic facies. **(a)** Location of the Fe duricrust profile in a Brazilian landscape, **(b)** distinct horizons of the profile, **(c)** pisolitic facies, **(d)** SEM (backscattered electrons) picture of the internal structure of a pisolite, and **(e)** contrasting compositional variation from the core to cortex. The white line in the SEM image in **(d)** indicates the transect analyzed and shown in **(e)**.

Rietveld refinements of the multiphase XRD patterns were performed with the FullProf software (Rodriguez-Carvajal, 1993) and included hematite, goethite, kaolinite, and anatase as mineral phases. Starting crystal structure data were taken from Finger and Hazen (1980), Gualtieri and Venturelli (1999), Bish and Von Dreele (1989), and Howard et al. (1991), respectively. Scale factors, cell parameters, isotropic pseudo-Voigt line-profile functions (Thompson–Cox–Hastings), and overall B factors were first refined for the four phases. The peak widths were significantly larger than the instrument resolution ($\sim 0.1^\circ\ 2\theta$). The instrumental resolution function (IRF) was determined over the 2θ range measured from the LaB6 crystallographic standard Rietveld refinement. Assuming that the Lorentzian part of the peak

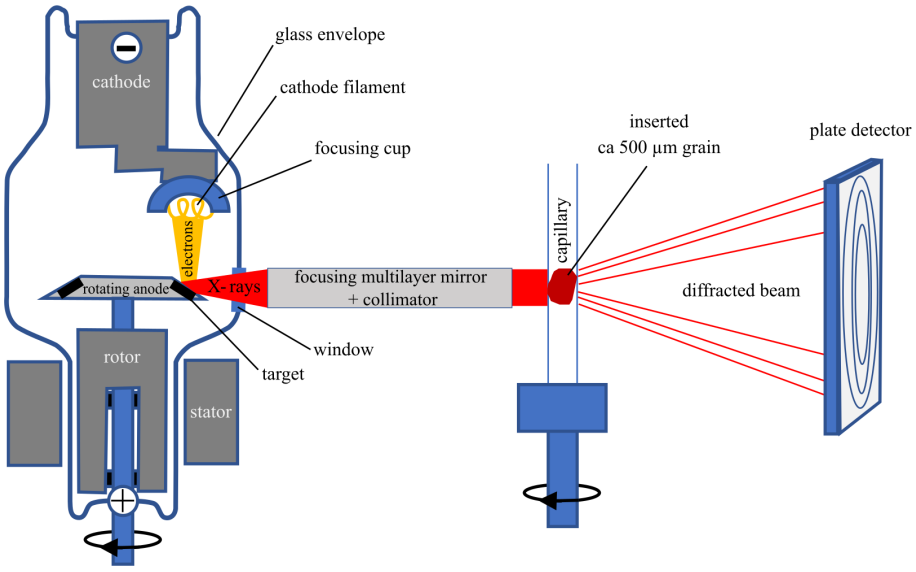

Figure 2. Diagram (not to scale) of the rotating anode X-ray diffraction device. Samples are inserted in a borosilicate glass capillary and rotated during the X-ray data collection by an image plate detector at a distance of 200 mm from the sample. A microfocused beam is provided by the multilayer mirror (78 µm) and the in-house-made collimator.

broadening is preferentially due to size effect and the Gaussian part to the microstrain, Lorentzian isotropic size (Y) and Gaussian isotropic strain (U) parameters were refined taking into account the IRF. Then, to improve the fits, anisotropic refinements of size parameters were carried out for hematite, goethite, and kaolinite. Regarding hematite, the anisotropic peak broadening has been modeled as a linear combination of spherical harmonics, and every coefficient was refined. This is used to calculate the average apparent sizes in the reciprocal lattice directions corresponding to every fitted Bragg reflection by applying Scherrer's formula (Klug and Alexander, 1974). In order to reduce the number of parameters to refine, we used a needle shape model elongated along the b axis for the goethite and a simplified model of platelet shape perpendicular to the c axis for the kaolinite. Regarding needle-like coherent domain, the obtained value is LorSiz $=$ SZ $\times \sin(\Phi)$, where SZ is the refined parameter and Φ is the acute angle between the scattering vector (h,k,l) and the vector defining the needle shape of domains. For platelet coherent domains, LorSiz is assumed to be of the form LorSiz $=$ SZ $\times \cos(\Phi)$, where SZ is the refined parameter and Φ is the acute angle between the scattering vector (h,k,l) and the vector defining the platelet shape of domains.

The weight percentage (wt %) ratio of the main phases was determined from Rietveld analysis of XRD_rotat and XRD_synch patterns of the powders (only XRD_rotat) and grains, following classical quantitative mineralogy procedures assuming a sum of mineral weight fractions equal to 1 (Snyder and Bish, 1989). When possible, Al^{3+} for Fe^{3+} substitution rates in goethite and hematite of powder and grain samples were determined by applying the empirical formula of Schulze (1984) and Schwertmann et al. (1979) using c and a unit-cell parameter values for goethite and hematite, respectively. Occupancy factors for Al and Fe were also refined to improve the fit quality but not used for estimating Al substitution rate since occupancy factors can be significantly affected by non-stoichiometry in soil iron oxyhydroxides that typically form at low temperature (Stanjek and Schwertmann, 1992; Wolska and Schwertmann, 1993). Therefore, we have been able to compare XRD_rotat and XRD_synch data and evaluate the possibility of characterizing the mineralogy of grains prior to dating.

The undisturbed grains from the pisolitic core and cortex were subject to different exposure times (30, 60, 90 min) during XRD_rotat recording to find the best conditions for X-ray analysis and verify that (U−Th)/He dating was not biased by He diffusion.

2.4 (U−Th)/He geochronology analysis

The grains previously analyzed at different acquisition times by XRD_rotat were weighed, their size was measured, and they were encapsulated into a Nb tube. Four grains from each population without exposure to irradiation were also analyzed in order to verify the reliability of our results. Grains of ca. 500 µm size sampled from a larger hematite or goethite environment were selected implying no significant natural He losses by alpha ejection (Farley et al., 1996). We considered then that the He lost by alpha ejection is compensated by alpha implantation from neighboring hematite or goethite mass. The aliquots were dated by the (U−Th)/He method at the GEOPS, Paris-Saclay University, France, following the protocols described in Allard et al. (2018) and Gautheron et

al. (2021). The Nb tubes were heated using a diode laser, and color image analysis of visible light emission was controlled with a camera in order to have a heating temperature below 1000 °C to avoid any U loss by volatilization (Vasconcelos et al., 2013; Hofmann et al., 2020). The ^{4}He content of the encapsulated grains was analyzed using a Pfeiffer Prisma Quadrupole mass spectrometer. More details can be founded in Gautheron et al. (2021). Afterward, grains inside Nb tubes were dissolved by adding 50 µL of 5 N HNO_3 containing ^{235}U, ^{230}Th, and ^{149}Sm; 50 µL of 5N HNO_3; 400 µL of 40 % concentrated HCl; and 100 µL of 38 % HF into 5 mL PFA capped vials (Savillex). The tightly closed vials were heated at about 100 °C overnight. The opened-cap vials were then placed on a hot plate at 100 °C for 2 h for complete evaporation. Then, a 1.9 mL volume of 1 N HNO_3 was added into the vial, and the solution was heated at 100 °C to reflux for 2 h. After cooling, 1.5 mL of the solution was taken and diluted with 1 N HNO_3 to reach a total volume of 3.4 mL, and a volume of 3 mL was sampled for analysis. Finally, ^{238}U, ^{232}Th, and ^{147}Sm contents were obtained by using a high-resolution inductively coupled plasma mass spectrometer (HR-ICP-MS; ELEMENT XR – Thermofisher Scientific). An analytical error of 5 % at 1σ is expected for the two-step analysis based on Durango apatite dating uncertainties associated with the analysis made in parallel to the goethite.

For goethite and hematite grains, a correction related to He loss, which is associated with the polycrystalline nature of goethite and hematite samples, was applied. For goethite, we used the recommendation of Bassal et al. (2022), where the He loss correction is dependent on the alpha recoil damage dose, calculated with the U–Th–Sm content and the (U−Th)/He age or the Al content. In this case, we used a correction of 15 ± 10 % as the goethite grains are characterized by an alpha damage dose of $\sim 4 \times 10^{14}\,\alpha\,g^{-1}$, and the Al content is < 10 % (Table 1). By contrast, for the mixing of hematite and goethite, we applied a correction factor of 10 % with an associated error of 10 %, which means the correction factor for pure hematite and goethite (Heller et al., 2022).

3 Results and discussion

3.1 Morphological description

The ferruginous duricrust profile of the studied site (see Fig. 1a for location) comprises a ferruginous duricrust stricto sensu (~ 4 m) transitioning upwards to a pisolite-rich (~ 1 m) and nodular indurated zone (~ 0.3 m) (Fig. 1b). The pisolites are well-formed, irregular in size and shape, and range from 5 to 10 mm in diameter (Fig. 1c). They are linked together by a matrix composed of goethite, kaolinite, and quartz (Nahon, 1976; Tardy and Nahon, 1985; Tardy, 1993). The pisolites present a concentric yellow-brown cortex that develops at the boundary of the purple-red core with a ferruginized zone (i.e., transition zone) between them. The well-developed concentric cortex presents an alternation of light and dark banded zones (Fig. 1d), where the light rings contain a higher Al and Si than Fe content (Fig. 1e), as often observed for pisolites from duricrusts (Nahon, 1976; McFarlane, 1983; Amouric et al., 1986; Anand and Gilkes, 1987).

3.2 XRD analysis of the core and cortex from the pisolitic facies

3.2.1 Rotating anode XRD patterns

Various assays of the XRD_rotat acquisition of grain samples from both pisolitic core and cortex were carried out using 30, 60, and 90 min exposure times in order to evaluate the quality of signal to noise in XRD patterns and to question the influence on He loss by diffusion and (U−Th)/He age. The XRD_rotat patterns of all samples were similar with a significantly high signal-to-noise ratio (Fig. S2). In addition, the excellent quality of the XRD_rotat patterns is clearly evidenced by comparing standard XRD on capillaries for the grain and the powder samples (Fig. S1). In particular, a 15 h collection pattern on a grain does not exhibit significant diffraction peaks. A 60 min exposure time was chosen for XRD_rotat as it provided good quality patterns for Rietveld refinement analysis.

The XRD_rotat patterns for grain and powder samples from the pisolitic core and cortex are shown in Fig. 3, with assigned mineral contributions. The grain and powder XRD patterns were predominantly similar, indicating that both types of sample preparation could be used to analyze the mineralogical composition for small amounts of sample (Fig. 3). However, the intensity of some peaks appears different for powder and grain samples, suggesting that their mineralogical content may not be fully equivalent. Indeed, the core sample shows a relative intensity of hematite (Hm) peaks slightly greater in the grain pattern than in the powder preparation (Fig. 3). This indicates a heterogeneous Hm content in the selected core facies at micron scale and strongly justifies the benefit of analyzing the mineralogy of an individual grain before (U−Th)/He geochronological analysis. Finally, we attest that XRD_rotat provides quality patterns on isolated ca. 500 µm grains without perturbation. In these conditions, the grain can then be exposed to a next-step analysis with no risk of data bias.

The XRD_rotat patterns indicate that hematite and goethite are present in the pisolitic core, whereas goethite and kaolinite are present in the cortex (Fig. 3). Although with a weak concentration, kaolinite is revealed by the peaks at 5.69 and 11.37° 2θ (Dixon and Weeds, 1989), which are not observed in the pisolitic core pattern. The absence of kaolinite in the pisolitic core is often related to its epigenetic replacement by hematite, which becomes more aluminous with the progressive dissolution of kaolinite (Nahon, 1976; Didier, 1983; Didier et al., 1983; Tardy and Nahon, 1985; Ambrosi et al., 1986). The reflection peak at 22.2° 2θ related to (204)

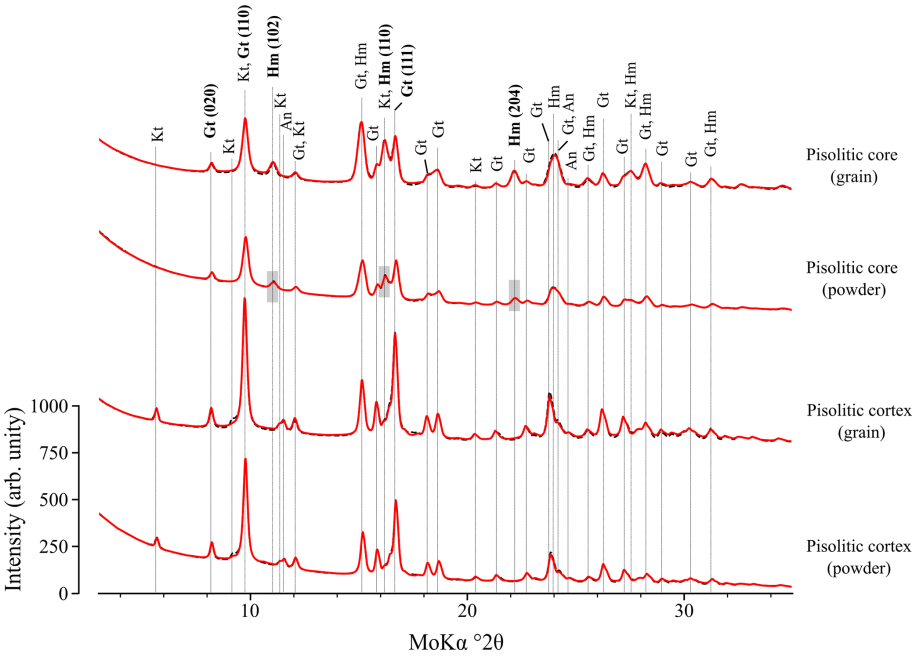

Figure 3. Rotating anode XRD patterns (60 min exposure time) for grain and powder samples from the pisolitic core and cortex of the ferruginous duricrust. Gt: goethite; Hm: hematite; Kt: kaolinite; and An: anatase. Note that the quality of the grain pattern is similar to that of the powder pattern. The red line represents the Rietveld fit, and the dashed black line is the experimental pattern. Grey areas correspond to isolated Hm peaks that vary between grain and powder patterns.

hematite was not observed in the XRD_rotat patterns of the pisolitic cortex, regardless of the sample preparation method, indicating a low amount or absence of hematite, as confirmed by the Rietveld refinement (Table 1). The mineralogical composition of the pisolitic core and cortex is consistent with previous studies (Didier et al., 1985; Amouric et al., 1986; Tardy, 1993).

In the grains, the weight percentage ratio of the main phases indicates that the pisolitic core contains 41 % of hematite, while the pisolitic cortex is predominantly composed of goethite (i.e., 95 %) (Table 1). The mean coherent domain (MCD) size from XRD_rotat is ca. 15 nm for core goethite, ca. 12 nm for the core hematite, and ca. 23 nm for the cortex goethite of grain samples (Table 1). The MCD sizes for goethite and hematite crystals are in agreement with those reported for other studies, with ranges within 10–40 nm for goethite and from 4–10 nm for hematite (e.g., Tardy and Nahon, 1985; Amouric et al., 1986; Anand and Gilkes, 1987). Al^{3+} for Fe^{3+} substitution rate, determined according to Schulze (1984) for goethite and Schwertmann et al. (1979) for hematite, is 9 % in core goethite, 1 % in core hematite, and 4 % in cortex goethite of grain samples (Table 1), suggesting a decrease in Al^{3+} for Fe^{3+} substitution rate in goethite from the pisolitic core to cortex.

3.2.2 Synchrotron XRD patterns

The synchrotron X-ray diffraction (XRD_synch) patterns for the grain samples from the pisolitic core and cortex were similar to those obtained by XRD_rotat data concerning the signal-to-noise ratio and identified mineral phases (Fig. 4). As expected, the synchrotron XRD patterns show a better resolution of diffraction peaks than XRD_rotat (Figs. 3 and 4). This can be related to the monochromatic wavelength of the incident synchrotron radiation and higher brilliance, which is useful for identifying minor constituents in a sample and particles of small size (Lombi and Susini, 2009; Tsao et al., 2013). Rietveld refinement provided a good fit for all the peaks, except for those corresponding to kaolinite because stacking disorder is not accounted for by the code (Fig. 4).

The weight percentage (wt %) ratio of the main phases from XRD_synch data is consistent with that determined with the XRD_rotat pattern (Table 1): a difference of 9 % is observed in the core grain and ≤ 1 % for the cortex grain. In addition, the MCD sizes were quite similar for both XRD data sources (Table 1). Al^{3+} for Fe^{3+} substitution rates in goethite for core and cortex samples were 12 % and 11 %, respectively. For the hematite core it was 7 %. These values are higher than those observed from XRD_rotat (Table 1).

Despite the different settings between XRD_rotat and XRD_synch, both methods are suitable for investigating the mineralogical composition of supergene phases in small sample mass (ca. 500 µm size). The XRD_rotat, available

Table 1. Mineralogical parameters determined for the core and cortex samples by Rietveld refinement of XRD_rotat (60 min exposure time) and XRD_synch patterns: weight percentage (wt %) ratio of the main phases (numbers between parentheses are absolute errors), mean coherent domain sizes of the hematite and goethite, and Al^{3+} for Fe^{3+} substitution rate in goethite and hematite.

Sample	Hm	Gt	Kt	An	MCD[a]		Al[b]	
	wt %	wt %	wt %	wt %	Gt	Hm	Gt	Hm
					nm		% mol	
XRD_rotat								
Core grain	41 (3.8)	59 (4.9)	0	0	15	12	9	1
Core powder	29 (4.7)	71 (7.1)	0	0	15	12	9	1
Cortex grain	0.3 (0.2)	95 (3.5)	2.7 (0.3)	2.5 (0.4)	23	[c]	4	[c]
Cortex powder	0.6 (0.5)	92 (4.6)	5.9 (1.3)	1.9 (0.5)	27	[c]	4	[c]
XRD_synch								
Core grain	32 (0.4)	68 (1.0)	0	nd	16	18	12	7
Cortex grain	0.7 (0.1)	94 (1.0)	5.3 (0.3)	nd	30	[c]	11	[c]

[a] Mean coherent domain sizes according to Scherrer's formula; [b] isomorphic substitution of Fe^{3+} by Al^{3+} according to Schulze (1984) for goethite and Schwertmann et al. (1979) for hematite. Hm: hematite; Gt: goethite; Kt: kaolinite; An: anatase; nd: not determined; [c] absent.

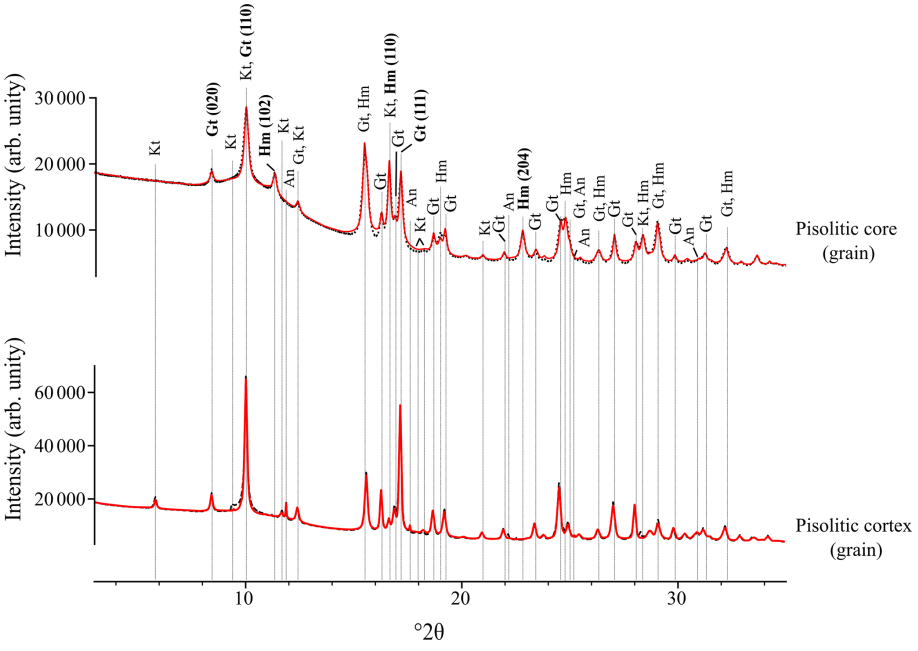

Figure 4. Synchrotron XRD patterns for grain samples from the pisolitic core and cortex. Gt: goethite; Hm: hematite; Kt: kaolinite; and An: anatase. The red line represents the Rietveld fit, and the dashed black line is the experimental pattern.

in laboratories, is powerful enough to analyze undisturbed grains that can be subsequently used for dating and thus appears much more appropriate than conventional XRD analysis that fails to analyze single grains (Fig. S1).

3.2.3 (U−Th)/He analysis

The effect of exposure time of XRD_rotat recording on apparent age for pisolitic core and cortex is shown in Fig. 5, and (U−Th)/He data are reported in Table 2. For each sample, there is no representative shift in age related to the acquisition time of mineralogical data: the results show a good reproducibility within the analytical uncertainty, i.e., 5 %. Figure 5 clearly shows that all the samples exhibit apparent age clusters including the 0 exposure point, supporting the idea that performing XRD_rotat mineralogical analysis prior to (U−Th)/He geochronological analysis is possible without impacting He content and age.

Table 2. Raw and corrected (U−Th)/He age for the investigated iron oxides and oxyhydroxides and Durango standard apatite.

Sample		Exposure time	Weight	^{4}He	Error	^{238}U	^{232}Th	^{147}Sm	^{4}He	Error	^{238}U	^{232}Th	^{147}Sm	eU	Th/U	Raw ages	Correction factor ± error	Corrected age	Error-corrected age
		min	µg	mol	mol	ng	ng	ng	nmol g^{-1}	nmol g^{-1}	ppm	ppm	ppm	ppm		Ma	%	Ma	Ma
Durango		0	29	6.70×10^{-13}	1.30×10^{-14}	0.69	14.12	1.27	22.69	0.05	23.4	480.2	43.2	139	20.6	30.7	0		
Durango		0	13	2.20×10^{-13}	4.40×10^{-15}	0.22	4.99	0.52	16.64	0.05	16.7	375.1	38.8	107	22.5	29.3	0		
Durango		0	29	5.30×10^{-13}	1.10×10^{-14}	0.53	11.44	1.12	17.98	0.02	17.9	388.0	38.1	111	21.6	30.4	0		
Durango		0	46	1.00×10^{-12}	2.10×10^{-14}	1.04	22.56	1.75	22.65	0.02	22.7	494.7	38.5	142	21.8	30.1	0		
Durango		0	64	1.90×10^{-12}	3.80×10^{-14}	2.03	39.66	3.82	29.68	0.05	31.6	618.0	59.5	180	19.6	31.0	0		
Durango		0	55	1.20×10^{-12}	2.30×10^{-14}	1.21	23.9	2.77	21.15	0.03	22.0	433.9	50.3	126	19.7	31.5	0		
Core	Hm + Gt	0	81	1.30×10^{-13}	2.60×10^{-15}	0.31	3.43	0.04	1.61	0	3.8	42.3	0.5	14	11.2	21.6	10 ± 10	23.8	2.2
Core	Hm + Gt	0	147	2.70×10^{-13}	5.40×10^{-15}	0.59	5.69	0.09	1.83	0	4.0	38.7	0.6	13	9.6	25.7	10 ± 10	28.3	2.6
Core	Hm + Gt	0	148	3.30×10^{-13}	6.60×10^{-15}	0.62	7.8	0.21	2.21	0	4.2	52.7	1.4	17	12.5	24.6	10 ± 10	27.1	2.5
Core	Hm + Gt	0	149	3.10×10^{-13}	6.10×10^{-15}	0.54	6.44	0.12	2.05	0	3.6	43.2	0.8	14	12.0	27.5	10 ± 10	30.3	2.8
Core	Hm + Gt	30	279	5.00×10^{-13}	1.00×10^{-14}	1.08	14.98	0.13	1.8	0	3.9	53.7	0.5	17	13.9	20.2	10 ± 10	22.2	2.0
Core	Hm + Gt	90	114	2.00×10^{-13}	3.90×10^{-15}	0.36	4.89	0.05	1.71	0	3.1	42.9	0.4	13	13.8	24.0	10 ± 10	26.4	2.4
Cortex	Gt	0	177	2.70×10^{-13}	5.40×10^{-15}	1.72	10.31	0.29	1.55	0.05	9.7	58.3	1.7	24	6.0	12.2	15 ± 10	14.0	1.2
Cortex	Gt	0	138	2.30×10^{-13}	4.60×10^{-15}	1.47	9.79	0.42	1.68	0.01	10.7	70.9	3.1	28	6.6	11.4	15 ± 10	13.1	1.1
Cortex	Gt	0	136	2.00×10^{-13}	4.00×10^{-15}	1.41	8.6	0.28	1.48	0.00	10.4	63.2	2.1	26	6.1	10.8	15 ± 10	12.4	1.1
Cortex	Gt	0	145	2.60×10^{-13}	5.20×10^{-15}	1.76	10.64	0.33	1.79	0.00	12.2	73.4	2.3	30	6.0	11.2	15 ± 10	12.9	1.1
Cortex	Gt	30	36	1.60×10^{-14}	3.10×10^{-16}	0.12	0.58	0.02	0.44	0.00	3.3	16.2	0.6	7	4.9	11.3	15 ± 10	13.0	1.1
Cortex	Gt	60	48	6.80×10^{-14}	1.40×10^{-15}	0.58	3.12	0.08	1.42	0.01	12.2	64.9	1.8	28	5.3	9.5	15 ± 10	10.9	1.0
Cortex	Gt	90	197	3.40×10^{-14}	6.80×10^{-16}	2.05	12.1	0.34	1.77	0.04	10.4	61.4	1.7	25	5.9	13.2	15 ± 10	15.2	1.3

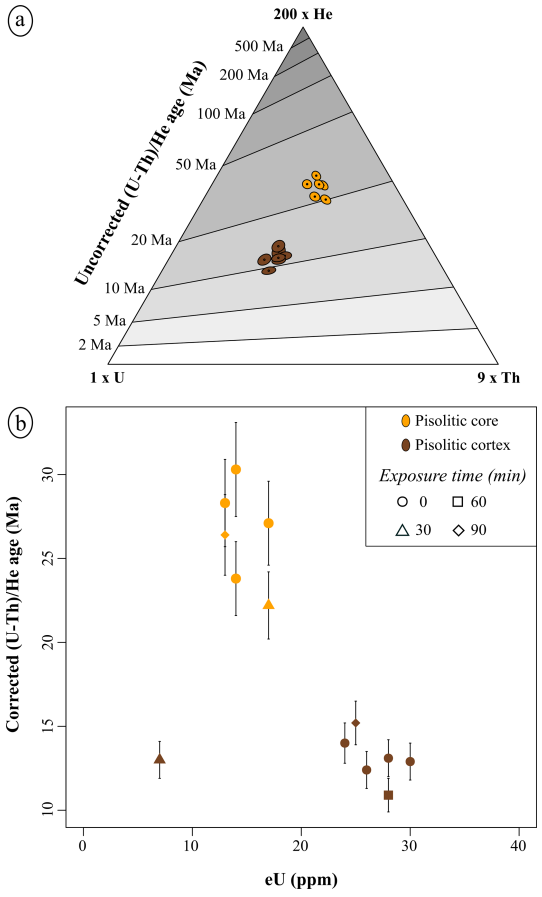

Figure 5. (U−Th)/He data. **(a)** Ternary diagram indicating the He–Th–U concentrations and the uncorrected (U−Th)/He ages (Ma) for pisolitic core and cortex obtained in the R environment using the *Helioplot* function (Vermeesch, 2010); and **(b)** evolution of the corrected (U−Th)/He age as a function of the effective uranium content ($eU = U + 0.238 \times Th + 0.0012 \times Sm$: Gastil et al., 1967; Cooperdock et al., 2019).

U and Th concentrations clearly differ between the pisolitic core and cortex, with higher values of both elements occurring in the pisolitic cortex. This suggests a relative U enrichment during the weathering of the Fe-oxides and oxyhydroxides from the core (Fig. 5). A grain from the pisolitic cortex (with 30 min exposure) contains lower U and Th concentrations than other grains (Fig. 5b), which can be explained by small differences between grains, as often occurs for grains of supergene minerals belonging to the same population (e.g., Vasconcelos et al., 2013; Monteiro et al., 2014; Riffel et al., 2016; Heller et al., 2022). Nevertheless, such a difference does not influence the age when compared to the other grains of the same facies at the millimeter scale (Fig. 5b).

Corrected (U−Th)/He ages for the pisolitic core range from 30 ± 2.8 to 22 ± 2.0 Ma and pisolitic cortex from 15 ± 1.3 to 11 ± 1.0 Ma (Table 2). The apparent age reveals that the pisolitic core is older than the pisolitic cortex, which is in full agreement with the model that takes into account the development of pisolites coming from different localities (e.g., Didier et al., 1983, 1985; Tardy and Nahon, 1985; Nahon and Tardy, 1992). It must be pointed out that the core age may be considered an average age of the hematite and goethite, which raises the question of the relative age of hematite and goethite in the core. This remains undetermined. Indeed, although MCD sizes and Al^{3+} for Fe^{3+} substitution rate in goethite from the core and cortex indicate that they formed in different conditions (Table 1), we have no constraint on the age of the core goethite. According to the (U−Th)/He age of the pisolitic core, a first formation episode of ferruginous duricrusts at the Alto Paranaíba region (Minas Gerais State, Brazil) occurred at, or before, the Oligocene, which indicates a period of optimal climate conditions in the study area, as already reported in a surrounding area (Monteiro et al., 2014, 2018). Our results indicate, in addition, that a secondary weathering process took place from the middle Miocene (∼ 15 to 11 Ma) (Table 2). More specifically, the Monteiro et al. (2014, 2018) studies provide age histograms covering a large period within the Cenozoic and exhibit a continuous occurrence of data in the short time interval revealed in our study. Other studies also identified distinct weathering episodes in Brazilian territory (e.g., Riffel et al., 2016; Allard et al., 2018; Vasconcelos et al., 2019). However, additional data are needed to further discuss the evolution of the studied duricrust and to relate its evolution to paleoclimates.

4 Conclusions

Mineralogy of supergene phases from core and cortex of a pisolitic facies can be explored on submillimetric (≤ 500 µm) single grains by XRD_rotat, which is a non-destructive method, yielding high-quality patterns, while standard XRD is not relevant. Rietveld refinement outputs such as phase concentrations and mean coherent domain sizes showed results consistent with XRD_synch. The grains analyzed by XRD_rotat do not exhibit X-ray exposure effects, and they are then suitable for further analysis such as (U−Th)/He dating. This approach could potentially be applied to other mineral parageneses (e.g., Mn-oxides, jarosites) prior to dating.

Although investigated over a small series of grains, corrected (U−Th)/He ages of pisolitic core ranging from ∼ 30 to 22 Ma revealed that a first formation episode of ferruginous duricrusts at the Alto Paranaíba region (Minas Gerais State, Brazil) occurred at or before the Oligocene. A subsequent phase associated with a secondary weathering formation process took place from the middle Miocene, which is highlighted by the formation of the goethitic pisolitic cortex. Therefore, the apparent (U−Th)/He age reveals that the pisolitic core is older than the pisolitic cortex, agreeing with

the model previously proposed for the development of pisolites in duricrusts.

Data availability. All data generated or analyzed during this study are included in this paper or its Supplement.

Supplement. The supplement related to this article is available online at: https://doi.org/10.5194/ejm-35-383-2023-supplement.

Author contributions. KPPM, TA, CG, and GM conceptualized the research and designed the methodology. KPPM carried out laboratory analysis and data interpretation. BB supported laboratory analysis including Rietveld refinement. LD and RPJ participated in mineralogical and (U−Th)/He analysis, respectively. PVT acquired the financial support for the project. KPPM, TA, and CG wrote the manuscript, integrated contributions from all co-authors, and made corrections to the revised version of the manuscript.

Competing interests. The contact author has declared that none of the authors has any competing interests.

Disclaimer. Publisher's note: Copernicus Publications remains neutral with regard to jurisdictional claims in published maps and institutional affiliations.

Acknowledgements. This research was funded by the São Paulo Research Foundation – FAPESP (grant nos. 2017/20788-2; 2017/22292-4; 2019/10708-7). This study was also financed in part by the Coordination for the Improvement of Higher Education Personnel (CAPES) – Finance Code 001. Thanks to the National Council for Scientific and Technological Development (CNPq) for the research grant to Pablo Vidal-Torrado (301818/2017-7). We thank Jessica Brest for help with sample preparation and Thierry Roisnel for fruitful discussions about Rietveld refinements. In the framework of the CNRS RÉCIPROCS network, this work has been accepted for synchrotron beamtime by the SOLEIL scientific proposal committee (BAG proposal 20191509). The authors would like to thank Erik Elkaïm for his help on CRISTAL beamline. We also thank Imène Esteve, Stéphanie Delbrel, and Béatrice Doisneau, who are working at the scanning electron microscope (SEM) of the Institut de Minéralogie, de Physique des Matériaux et de Cosmochimie (IMPMC – Sorbonne Université). It is supported by Région Ile de France grant SESAME 2006 no. I-07-593/R, INSU-CNRS, INP-CNRS, University Pierre et Marie Curie – Paris 6, and by the French National Research Agency (ANR) grant no. ANR-07-BLAN-0124-01. (U−Th)/He analyses were funded by the RECA ANR-17-CE01-0012-01 project. We thank the editor Elisabetta Rampone, Klaus Mezger, Florian Hofmann, and one anonymous review for the thoughtful comments that helped improve the manuscript.

Financial support. This research has been supported by the Fundação de Amparo à Pesquisa do Estado de São Paulo (grant nos. 2017/20788-2, 2017/22292-4, and 2019/10708-7) and the Agence Nationale de la Recherche (grant no. RECA ANR-17-CE01-0012-01).

Review statement. This paper was edited by Klaus Mezger and reviewed by Florian Hofmann and one anonymous referee.

References

Aleva, G. J. J. (Ed.): Laterites: Concepts, Geology, Morphology and Chemistry, International Soil Reference and Information Centre, Wageningen, the Netherlands, 1994.

Allard, T., Gautheron, C., Riffel, S. B., Balan, E., Soares, B. F., Pinna-Jamme, R., Derycke, A., Morin G., Bueno, G. T., and Nascimento, N.: Combined dating of goethites and kaolinites from ferruginous duricrusts. Deciphering the Late Neogene erosion history of Central Amazonia, Chem. Geol., 479, 136–150, https://doi.org/10.1016/j.chemgeo.2018.01.004, 2018.

Ambrosi, J. P., Nahon, D., and Herbilon, A. J.: The epigenetic replacement of kaolinite by hematite in laterite. Petrographic evidence and the mechanisms involved, Geoderma, 37, 283–294, https://doi.org/10.1016/0016-7061(86)90030-3, 1986.

Amouric, M., Baronneta, A., Nahon, D., and Didier, P.: Electron microscopic investigations of iron oxyhydroxides and accompanying phases in lateritic iron-crust pisolites, Clay. Clay Miner., 34, 45–52, 1986.

Anand, R. R. and Gilkes, R. J.: Variations in the properties of iron oxides within individual specimens of lateritic duricrust, Aust. J. Soil Res., 25, 287–302, https://doi.org/10.1071/SR9870287, 1987.

Balout, H., Roques, J., Gautheron, C., Tassan-Got, L., and Mbongo-Djimbi, D.: Helium diffusion in pure hematite (a-Fe_2O_3) for thermochronometric applications: A theoretical multi-scale study, Comput. Theor. Chem., 1099, 21–28, https://doi.org/10.1016/j.comptc.2016.11.001, 2017.

Bassal, F., Heller, B., Roques, J., Balout, H., Tassan-Got, L., Allard, T., and Gautheron, C.: Revealing the radiation damage and Al-content impacts on He diffusion in goethite, Chem. Geol., 611, 121118, https://doi.org/10.1016/j.chemgeo.2022.121118, 2022.

Beauvais, A. and Chardon, D.: Modes, tempo, and spatial variability of Cenozoic cratonic denudation: The West African example, Geochem. Geophy. Geosy., 14, 1590–1608, https://doi.org/10.1002/ggge.20093, 2013.

Bish, D. L. and Post, J. E.: Quantitative mineralogical analysis using the Rietveld full-pattern fitting method, Am. Mineral., 78, 932–940, 1993.

Bish, D. L. and Von Dreele, R. B.: Rietveld refinement of non-hydrogen atomic positions in kaolinite, Clay. Clay Miner., 37, 289–296, https://doi.org/10.1346/CCMN.1989.0370401, 1989.

Cooperdock, E. H. G., Ketcham, R. A., and Stockli, D. F.: Resolving the effects of 2-D versus 3-D grain measurements on apatite (U−Th)/He age data and reproducibility, Geochronology, 1, 17–41, https://doi.org/10.5194/gchron-1-17-2019, 2019.

CPRM – SERVIÇO GEOLÓGICO DO BRASIL: Mapa geológico do Estado de Minas Gerais – 1 : 1.000.000, CPRM, Belo Horizonte, 2014.

Deng, X. D., Li, J. W., and Shuster, D. L.: Late Mio-Pliocene chemical weathering of the Yulong porphyry Cu deposit in the eastern Tibetan Plateau constrained by goethite (U−Th)/He dating: Implication for Asian summer monsoon, Earth Planet. Sc. Lett., 472, 289–298, https://doi.org/10.1016/j.epsl.2017.04.043, 2017.

Didier, P.: Paragenèses à oxydes et hydroxydes de fer dans les bauxites et les cuirasses ferrugineuses, Thèse 3e cycle, Univ. Poitiers, France, 150 pp., 1983.

Didier, P., Nahon, D., Fritz, B., and Tardy, Y.: Activity of water as a geochemical controlling factor in ferricretes. A thermodynamic model in the system: kaolinite Fe-Al-oxihydroxides, Sei. Géol. Mérn., 71, 35–44, 1983.

Didier, P., Perret, D., Tardy, Y., and Nahon, D.: Equilibres entre kaolinites ferrifères, goethites alumineuses et hématites alumineuses dans les systèmes cuirasses rôle de l'activité de l'eau et de la taille des pores, Sci. Géol. Bull., 38, 383–397, 1985.

Dixon, J. B. and Weeds, S. B. (Eds.): Minerals in Soil Environments, Soil Science Society of America, Madison, WI, https://doi.org/10.2136/sssabookser1.2ed, 1989.

Evenson, N. S., Reiners, P. W., Spencer, J. E., and Shuster, D.: Hematite and Mn oxide (U−Th)/He dates from the Buckskin-Rawhide detachement system, western Arizona: gaining insights into hematite (U−Th)/He systematics, Am. J. Sci., 314, 1373–1435, https://doi.org/10.2475/10.2014.01, 2014.

Farley, K. A.: Helium diffusion parameters of hematite from a single-diffusion-domain crystal, Geochim. Cosmochim. Ac., 231, 117–129, https://doi.org/10.1016/j.gca.2018.04.005, 2018.

Farley, K. A. and Flowers, R.: (U−Th)/Ne and multidomain (U−Th)/He systematics of a hydrothermal hematite from Eastern Grand Canyon, Earth Planet. Sc. Lett., 359–360, 131–140, https://doi.org/10.1016/j.epsl.2012.10.010, 2012.

Farley, K. A., Wolf, R. A., and Silver, L. T.: The effects of long alpha-stopping distances on (U−Th)/He ages, Geochim. Cosmochim. Ac., 60, 4223–4229, https://doi.org/10.1016/S0016-7037(96)00193-7, 1996.

Finger, L. W. and Hazen, R. M.: Crystal Structure and Isothermal Compression of Fe_2O_3, Cr_2O_3, and V_2O_3 to 50 Kbars, J. Appl. Phys., 51, 5362–5367, https://doi.org/10.1063/1.327451, 1980.

Gastil, R. G., Delisle, M., and Morgan, J. R.: Some effects of progressive metamorphism on zircons, Geol. Soc. Am. Bull., 78, 879–906, https://doi.org/10.1130/0016-7606(1967)78[879:SEOPMO]2.0.CO;2 , 1967.

Gautheron, C., Pinna-Jamme, R., Derycke, A., Ahadi, F., Sanchez, C., Haurine, F., Monvoisin, G., Barbosa, D., Delpech, G., Maltese, J., Sarda, P., and Tassan-Got, L.: Technical note: Analytical protocols and performance for apatite and zircon (U−Th)/He analysis on quadrupole and magnetic sector mass spectrometer systems between 2007 and 2020, Geochronology, 3, 351–370, https://doi.org/10.5194/gchron-3-351-2021, 2021.

Gautheron, C., Hueck, M., Ternois, S., Heller, B., Schwartz, S., Sarda, P., and Tassan-Got, L.: Investigating the Shallow to Mid-Depth ($>$ 100–300 °C) Continental Crust Evolution with (U−Th)/He Thermochronology: A Review, Minerals, 12, 563, https://doi.org/10.3390/min12050563, 2022.

Gualtieri, A. and Venturelli, P.: In situ study of the goethite-hematite phase transformation by real time synchrotron powder diffraction, Am. Mineral., 84, 895–904, https://doi.org/10.2138/am-1999-5-624, 1999.

Hammersley, A. P.: FIT2D: a multi-purpose data reduction, analysis and visualization program, J. Appl. Cryst., 49, 646–652, https://doi.org/10.1107/S1600576716000455, 2016.

Heim, J. A., Vasconcelos, P. M., Shuster, D. L., Farley, K. A., and Broadbent, G.: Dating paleochannel iron ore by (U−Th)/He analysis of supergene goethite, Hamersley province, Australia, Geology, 34, 173–176, https://doi.org/10.1130/G22003.1, 2016.

Heller, B. H., Riffel, S. B., Allard, T., Morin, G., Roig, J., Couëffe, R., Aertsgeerts, G., Derycke, A., Ansart, C., Pinna-Jamme, R., and Gautheron, C.: Reading the climate signals hidden in bauxite, Geochim. Cosmochim. Ac., 323, 40–73, https://doi.org/10.1016/j.gca.2022.02.017, 2022.

Hofmann, F., Reichenbacher B., and Farley, K. A.: Evidence for $>$ 5 Ma paleo-exposure of an Eocene-Miocene paleosol of the Bohnerz Formation, Switzerland, Earth Planet. Sc. Lett., 465, 168–175, https://doi.org/10.1016/j.epsl.2017.02.042, 2017.

Hofmann, F., Treffkorn, J., and Farley, K. A.: U-loss associated with laser-heating of hematite and goethite in vacuum during (U-Th) / He dating and prevention using high O_2 partial pressure, Chem. Geol., 532, 119350, https://doi.org/10.1016/j.chemgeo.2019.119350, 2020.

Howard, C. J., Sabine, T. M., and Dickson, F.: Structural and thermal parameters for rutile and anatase, Acta Crystallogr. B, 47, 462–468, https://doi.org/10.1107/S010876819100335X, 1991.

Klug, H. P. and Alexander, L. E. (Eds.): X-ray Diffraction Procedures for Polycrystalline and Amorphous Materials, 2nd Edn., John Wiley & Sons, New York, 1974.

Lippolt, H. J., Leitz, M., Wernicke, R. S., and Hagedorn, B.: (Uranium + thorium) / helium dating of apatite: Experience with samples from different geochemical environments, Chem. Geol., 112, 179–191, https://doi.org/10.1016/0009-2541(94)90113-9, 1994.

Lombi, E. and Susini, J.: Synchrotron-based techniques for plant and soil science: opportunities, challenges and future perspectives, Plant Soil, 320, 1–35, 2009.

Marques, K. P. P., Santos, M., Peifer, D., Silva, C. L., and Vidal-Torrado, P.: Transient and relict landforms in a lithologically heterogeneous post-orogenic landscape in the intertropical belt (Alto Paranaíba region, Brazil), Geomorphology, 391, 107892, https://doi.org/10.1016/j.geomorph.2021.107892, 2021.

McFarlane, M. J.: Laterite and Landscape, Academic Press, London, 1976.

McFarlane, M. J.: Laterites, in: Chemical sediments and geomorphology, edited by: Goudie, A. S. and Pye, K., Academic Press, New York, 7–58, 1983.

Monteiro, H. S., Vasconcelos, P. M. P., Farley, K. A., Spier, C. A., and Mello, C. L.: (U−Th)/He geochronology of goethite and the origin and evolution of cangas, Geochim. Cosmochim. Ac., 131, 267–289, https://doi.org/10.1016/j.gca.2014.01.036, 2014.

Monteiro, H. S., Vasconcelos, P. M. P., and Farley, K. A.: A combined (U−Th)/He and cosmogenic ^{3}He record of landscape armoring by biogeochemical iron cycling, J. Geophys. Res.-Earth, 123, 298–323, https://doi.org/10.1002/2017JF004282, 2018.

Nahon, D.: Cuirasses ferrugineuses et encroûtements calcaires au Sénégal occidental et en Mauritanie, Mém. Sci. Géol. Strassbourg, 44, 232 pp., 1976.

Nahon, D.: Evolution of iron crusts in tropical landscapes, in: Rates of Chemical Weathering of Rocks and Minerals, edited by: Colman, S. M. and Dethier, D. P., Academic Press, New York, 169–191, 1986.

Nahon, D. and Tardy, Y.: The ferruginous laterites, in: Regolith exploration geochemistry in tropical and subtropical terrains, Handbook of exploration geochemistry, edited by: Butt, C. R. M. and Zeegerds, H., Elsevier, Amsterdam, 41–55, https://doi.org/10.1016/B978-0-444-89095-5.50010-9, 1992.

Nahon, D. B.: Introduction to the Petrology of Soils and Chemical weathering, John Wiley & Sons, New York, 1991.

Oliveira, P. E., Raczka, M., McMichael, C. N. H., Pinaya, J. L. D., and Bush, M. B.: Climate change and biogeographic connectivity across the Brazilian cerrado, J. Biogeogr., 47, 396–407, https://doi.org/10.1111/jbi.13732, 2020.

Ollier, C. D. and Sheth, H. C.: The High Deccan duricrusts of India and their significance for the "laterite" issue, J. Earth Syst. Sci., 117, 537–551, https://doi.org/10.1007/s12040-008-0051-9, 2008.

Riffel, S. B., Vasconcelos, P. M., Carmo, I. O., and Farley, K. A.: Goethite (U−Th)/He geochronology and precipitation mechanisms during weathering of basalts, Chem. Geol., 446, 18–32, https://doi.org/10.1016/j.chemgeo.2016.03.033, 2016.

Rodriguez-Carvajal, J.: FullProf Program, Physica B, 192, 55–69, 1993.

Schulze, D. G.: The influence of aluminium on iron oxides. VIII – unit-cell dimensions of Al-substituted goethites and estimation of Al from them, Clay. Clay Miner., 32, 36–44, https://doi.org/10.1346/CCMN.1984.0320105, 1984.

Schwertmann, U., Fitzpatrick, R. W., Taylor, R. M., and Lewis, D. G.: The influence of aluminum on iron oxides. Part II. Preparation and properties of Al-substituted hematites, Clay. Clay Miner., 27, 105–112, https://doi.org/10.1346/CCMN.1979.0270205, 1979.

Shuster, D. L., Vasconcelos, P. M. P., Heim, J. A., and Farley, K. A.: Weathering geochronology by (U−Th)/He dating of goethite, Geochim. Cosmochim. Ac., 69, 659–673, https://doi.org/10.1016/j.gca.2004.07.028, 2005.

Shuster, D. L., Farley, K. A., Vasconcelos, P. M. P., Balco, G., Monteiro, H. S., Waltenberg, K., and Stone, J. O.: Cosmogenic 3He in hematite and goethite from Brazilian "canga" duricrust demonstrates the extreme stability of these surfaces, Earth Planet. Sc. Lett., 329–330, 41–50, https://doi.org/10.1016/j.epsl.2012.02.017, 2012.

Snyder, R. L. and Bish, D. L.: Quantitative analysis, in: Modern Powder Diffraction, Rev. Miner., 20, edited by: Bish, D. L. and Post, J. E., Mineralogical Society of America, Washington, 101–144, 1989.

Stanjek, H. and Schwertmann, U.: The influence of aluminium on iron oxides. XVI: Hydroxyl and aluminum substitution in synthetic hematites, Clay. Clay Miner., 40/3, 347–354, https://doi.org/10.1346/CCMN.1992.0400316, 1992.

Tardy, Y. (Ed.): Pétrologie des latérites et des sols tropicaux, Masson, Paris, 1993.

Tardy, Y. and Nahon, D.: Geochemistry of laterites, stability of Al-goethite, Al-hematite and Fe^{3+}-kaolinite in bauxites and ferricretes: an approach of the mechanism of concretion formation, Am. J. Sci. 285, 865–903, https://doi.org/10.2475/ajs.285.10.865, 1985.

Tardy, Y. and Roquin, C. (Eds.): Dérive des continents. Paléoclimats et altérations tropicales, Éditions BGM, Orléans, 1998.

Théveniaut, H. and Freyssinet, P.: Paleomagnetism applied to lateritic profiles to assess saprolite and duricrust formation processes: the example of Mont Baduel profile (French Guiana), Palaeogeogr. Palaeocl., 148, 209–231, https://doi.org/10.1016/S0031-0182(98)00183-7, 1999.

Théveniaut, H. and Freyssinet, P.: Timing of lateritization on the Guiana shield: synthesis of paleomagnetic results from French Guiana and Suriname, Palaeogeogr. Palaeocl., 178, 91–117, https://doi.org/10.1016/S0031-0182(01)00404-7, 2002.

Tsao, T., Chen, Y., Sheu, H., Tzou, Y., Chou, Y., and Wang, M.: Separation and identification of soil nanoparticles by conventional and synchrotron X-ray diffraction, Appl. Clay Sci., 85, 1–7, https://doi.org/10.1016/j.clay.2013.09.005, 2013.

Vasconcelos, P. M. and Carmo, I. D. O.: Calibrating denudation chronology through $^{40}Ar/^{39}Ar$ weathering geochronology, Earth-Sci. Rev., 179, 411–435, https://doi.org/10.1016/j.earscirev.2018.01.003, 2018.

Vasconcelos, P. M., Heim, J. A., Farley, K. A., Monteiro, H., and Waltenberg, K.: $^{40}Ar/^{39}Ar$ and (U−Th)/He – $^{4}He/^{3}He$ geochronology of landscape evolution and channel iron deposit genesis at Lynn Peak, Western Australia, Geochim. Cosmochim. Ac., 117, 283–312, https://doi.org/10.1016/j.gca.2013.03.037, 2013.

Vasconcelos, P. M., Farley, K. A., Stone, J., Piacentini, T., and Fifield, L. K.: Stranded landscapes in the humid tropics: Earth's oldest land surfaces, Earth Planet. Sc. Lett., 519, 152–164, https://doi.org/10.1016/j.epsl.2019.04.014, 2019.

Vermeesch, P.: HelioPlot, and the treatment of overdispersed (U−Th−Sm)/He data, Chem. Geol., 271, 108–111, https://doi.org/10.1016/j.chemgeo.2010.01.002, 2010.

Wolska, E. and Schwertmann, U.: The mecanism of solid solution formation between goethite and diaspore, Neues Jb. Miner. Monat., 5, 213–223, 1993.